

A potential progenitor for the Type Ic supernova 2017ein

Charles D. Kilpatrick, ^{1★} Tyler Takaro, ¹ Ryan J. Foley, ¹ Camille N. Leibler, ¹ Yen-Chen Pan, ¹ Randall D. Campbell, ² Wynn V. Jacobson-Galan, ¹ Hilton A. Lewis, ² James E. Lyke, ² Claire E. Max, ¹ Sophia A. Medallon ¹ and Armin Rest^{3,4}

Accepted 2018 July 23. Received 2018 July 7; in original form 2018 April 18

ABSTRACT

We report the first detection of a credible progenitor system for a Type Ic supernova (SN Ic), SN 2017ein. We present spectra and photometry of the SN, finding it to be similar to carbon-rich, low-luminosity SNe Ic. Using a post-explosion Keck adaptive optics image, we precisely determine the position of SN 2017ein in pre-explosion HST images, finding a single source coincident with the SN position. This source is marginally extended, and is consistent with being a stellar cluster. However, under the assumption that the emission of this source is dominated by a single point source, we perform point-spread function photometry, and correcting for line-of-sight reddening, we find it to have $M_{\rm F555W}=-7.5\pm0.2$ mag and $m_{\rm F555W}-m_{\rm F814W}=-0.67\pm0.14$ mag. This source is bluer than the main sequence and brighter than almost all Wolf-Rayet stars, however, it is similar to some WC+O- and B-star binary systems. Under the assumption that the source is dominated by a single star, we find that it had an initial mass of $55^{+20}_{-15} \rm{M}_{\odot}$. We also examined binary star models to look for systems that match the overall photometry of the pre-explosion source and found that the best-fitting model is an $80+48M_{\odot}$ close binary system in which the $80M_{\odot}$ star is stripped and explodes as a lower mass star. Late-time photometry after the SN has faded will be necessary to cleanly separate the progenitor star emission from the additional coincident emission.

Key words: stars: evolution – supernovae: general – supernovae: individual (SN 2017ein).

1 INTRODUCTION

In the past three decades, there have been over 20 detections of pre-explosion counterparts to core-collapse supernovae (SNe; for a review, see Smartt 2009). Most of these counterparts are red supergiant (RSG) progenitor stars of Type II-P SNe (SNe with a 'plateau' in their light curves consistent with recombination emission from an extended hydrogen envelope), which agrees with predictions from star formation and stellar evolution that suggest low-mass RSG progenitors stars should be relatively common.

There are, however, mixed results in finding the progenitor systems of other SN sub-types, with identified progenitor systems for some SNe IIn (SNe with narrow lines of hydrogen in their spectra, e.g. SNe 2005gl and 2009ip; Gal-Yam et al. 2007; Smith et al. 2010) and SNe IIb (SNe with transient hydrogen lines in their spectra, with progenitor star detections for SNe 1993J, 2008ax, 2011dh, 2013df, and 2016gkg; Aldering, Humphreys & Richmond 1994;

* E-mail: cdkilpat@ucsc.edu

Woosley et al. 1994; Crockett et al. 2008; Dessart et al. 2011, 2015; Maund et al. 2011; Van Dyk et al. 2014; Kilpatrick et al. 2017). The progenitor stars of SNe Ib/c (which have no hydrogen in their spectra, or helium in the case of SNe Ic) have been comparatively elusive and only one credible pre-explosion counterpart has been identified so far in the literature (the SN Ib iPTF13bvn; Cao et al. 2013).

In part, the paucity of pre-explosion SN counterparts for SNe Ib/c is because they only make up ~20 per cent of transients discovered in volume-limited surveys (e.g. LOSS; Li et al. 2000, 2011; Smith et al. 2011; Shivvers et al. 2017), and the incidence of SNe with deep, high-resolution pre-explosion imaging is even smaller. However, as more nearby SNe are discovered, especially those with pre-explosion *Hubble Space Telescope (HST)* imaging, the growing sample of upper limits on SN Ic progenitor systems in particular has placed strong constraints on predictions from stellar evolution and SN explosion models (with deep limits on counterparts for SNe 2002ap, 2004gt, and 2007gr; Gal-Yam et al. 2005; Crockett et al. 2007, 2008; Maund & Ramirez-Ruiz 2016). This evidence suggests that some non-RSG SN progenitor stars are either intrinsically less

¹Department of Astronomy and Astrophysics, University of California, Santa Cruz, CA 95064, USA

²W. M. Keck Observatory, 65-1120 Mamalahoa Hwy., Kamuela, HI 96743, USA

³Space Telescope Science Institute, 3700 San Martin Drive, Baltimore, MD 21218, USA

⁴Department of Physics and Astronomy, Johns Hopkins University, 3400 North Charles Street, Baltimore, MD 21218, USA

luminous than RSGs or heavily obscured by dust in the *HST* optical bands typically available for pre-explosion imaging. These stars may highly stripped by stellar winds, and although they may be comparable in luminosity to RSGs, their SEDs peak predominantly in the ultraviolet (and outside of optical or infrared bands in which pre-explosion imaging is typically available; for a review of SN Ib/c progenitor studies see Eldridge et al. 2013). Dust obscuration is a distinct possibility for high-mass SN progenitor stars, as some high-mass RSGs are observed to have optically thick circumstellar dust (e.g. SN 2012aw; Kochanek, Khan & Dai 2012). In addition, high-mass SN progenitor stars ought to explode promptly, perhaps close to the dusty environments where they form (see e.g. analysis of SN environments in Kuncarayakti et al. 2013; Galbany et al. 2016, 2017).

Because SNe Ic are the explosions of massive stars without significant hydrogen or helium in their outer layers, their progenitor star must be significantly stripped by stellar winds or a companion star. Highly stripped Wolf–Rayet (WR) stars are therefore good candidates for SN Ic progenitor stars (Yoon, Woosley & Langer 2010; Yoon et al. 2012; Yoon 2017). WR stars undergo radiatively driven mass loss at rates exceeding 10⁵M⊙yr⁻¹ (although exact massloss rates are highly uncertain; Maeder & Meynet 1987; Hamann, Koesterke & Wessolowski 1995; Smith 2014), and so observational and theoretical evidence suggest that some pre-SN WR stars ought to be hydrogen- and helium-deficient (Podsiadlowski, Rappaport & Pfahl 2002; Woosley, Langer & Weaver 1993; Steiner & Oliveira 2005).

However, radiatively driven winds are highly metallicitydependent and WR stars tend to form in high-metallicity environments: indeed, the Small Magellanic Cloud exhibits a decreased WR-to-O-star ratio relative to Solar neighbourhood (Hainich et al. 2015). Predicted mass-loss rates for WR stars at Solar metallicities indicate that single WR stars may have high pre-SN masses (Meynet & Maeder 2005) and very few of these stars are predicted to be helium-poor (e.g. Yoon 2015a). This finding is in tension with predictions that they are SN Ic progenitor stars given SN Ic rates and their typical ejecta masses (Drout et al. 2011; Taddia et al. 2015). One alternative is that, if WR stars are a likely channel for producing SNe Ic, most SN progenitor systems are interacting binaries in which a WR star has been stripped by a companion. This hypothesis is supported by the fact that many late-type WR stars are observed to be in close binaries with O-type stars (e.g. WR 104; Tuthill, Monnier & Danchi 1999) as well as the fact that the overall binary fraction for Milky Way WR stars is 40 per cent (van der Hucht 2001). If SNe Ic mostly come from low-mass WR stars in close binaries or in dusty environments, this would explain their non-detection in optical pre-explosion imaging to date, and so examples with deep detection limits can be used to verify or rule out this possibility.

In this paper, we discuss the SN Ic 2017ein discovered in NGC 3938 on 2017 May 25 by Arbour (2017). Deep imaging starting 2 days before discovery and continuing for 2 weeks afterwards indicated that SN 2017ein rose quickly after discovery (Im et al. 2017), which suggests that it was discovered very soon after explosion.

Here, we report photometry, spectroscopy, and high-resolution adaptive optics imaging of SN 2017ein. We demonstrate that SN 2017ein is most consistent with carbon-rich SNe Ic, although the source exhibits strong Na₁ D lines at the redshift of NGC 3938 and is significantly reddened. We use relative astrometry between our high-resolution and pre-explosion imaging, we find a single, luminous, blue source consistent with being the progenitor system of SN 2017ein, although that source appears extended and may be a

blend of multiple point sources. By comparing this source to Galactic supergiants and evolutionary tracks, we investigate channels that could produce the SN 2017ein progenitor system.

While we were preparing this manuscript, Van Dyk et al. (2018) published another analysis of SN 2017ein and its pre-explosion imaging. The authors came to similar conclusions about the nature of SN 2017ein and its photometric and spectroscopic similarity to carbon-rich SNe Ic. They identified the same source in pre-explosion imaging as the potential progenitor system of SN 2017ein and concluded the SN likely had a very massive (>45 M_{\odot}) progenitor star.

Throughout this paper, we assume a distance to NGC 3938 of $m - M = 31.17 \pm 0.10$ (Tully et al. 2009) and Milky Way extinction of $A_V = 0.058$ (Schlafly & Finkbeiner 2011).

2 OBSERVATIONS

2.1 Archival data

We obtained archival imaging of NGC 3938 from the HST MAST Archive¹ from 2007 December 11 (Cycle 15, Proposal 10877, PI Li). The HST data were obtained with WFPC2 and consisted of two frames each of F555W and F814W totaling 2 \times 230 s and 2×350 s, respectively. We obtained the individual c0m frames, which had been calibrated with the latest reference files, including corrections for bias, dark current, flat-fielding, and bad-pixel masking. The images were combined using the DRIZZLEPAC² software package, which performs cosmic ray rejection, and final image combination using the Drizzle algorithm. The final drizzled images had a pixel scale of 0.10 arcsec, which is consistent with the native pixel scale of the WF2 array where SN 2017ein landed. Using these final drizzled images as a reference, we used dolphot on the individual WFPC2/c0m frames with parameters optimized for the WF arrays on HST/WFPC2. These parameters were typically those recommended for dolphot WFPC2 analysis,³ but with local measurements of the sky background and slightly larger aperture radius.4 This method is more accurate for faint sources in crowded fields and where non-uniform background emission can contaminate the PSFs for individual sources, as may be the case for SN 2017ein. Our combined HST image is shown in Fig. 1.

2.2 Adaptive optics imaging

We observed SN 2017ein in *H* band in imaging mode with the OH-Suppressing Infrared Imaging Spectrograph (OSIRIS; Larkin et al. 2006) on the Keck-I 10-m telescope in conjunction with the laser guide star adaptive optics (LGSAO) system on 2017 June 6. These data consisted of 2 individual frames each with 10 co-adds of 30s for an effective exposure time of 300s per frame or 600s total. The individual frames were corrected for pixel-to-pixel variations using a flat-field frame that was created from observations of a uniformly illuminated flat-field screen in the same instrumental setup and filter. We modelled and subtracted the sky background emission in each pixel by taking the median pixel value in a box centred on that pixel and with a width of 63 pixels (roughly 6 per cent the image size or

¹https://hla.stsci.edu/hla_faq.html

²http://drizzlepac.stsci.edu/

³http://americano.dolphinsim.com/dolphot

⁴i.e. FitSky = 2 and $img_RAper = 5.33$

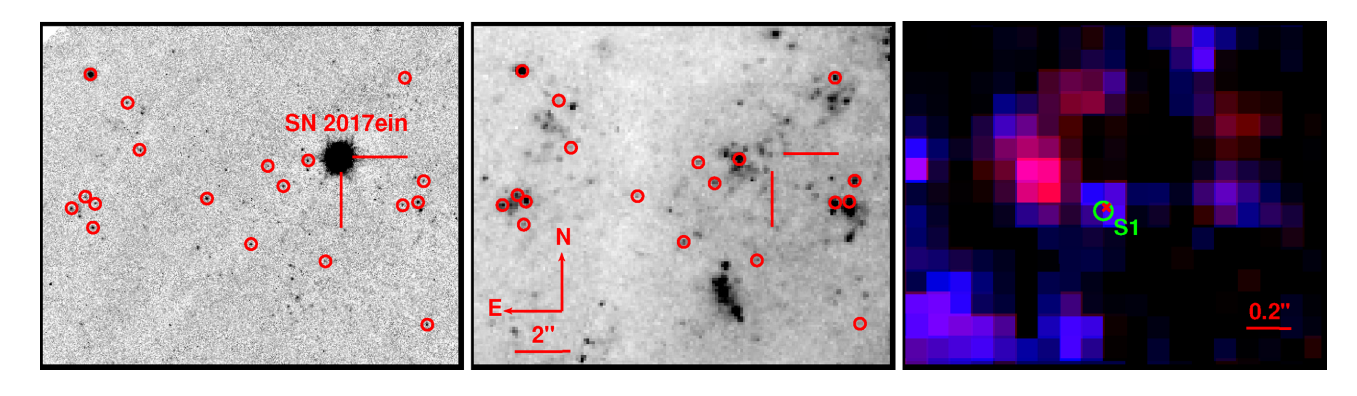


Figure 1. Left: Keck OSIRIS LGSAO *H*-band imaging of SN 2017ein. The SN is denoted by red tick marks and 18 point sources used for astrometry are circled in red. Middle: *HST* WFPC2 *F*814*W* reference image used for astrometry. The progenitor star is denoted and the same 18 point sources from the OSIRIS image are circled in red. Right: Red/blue (*F*555*W*/*F*814*W*) composite *HST*/WFPC2 image zoomed in on the location of the SN 2017ein counterpart. The location of SN 2017ein derived from relative astrometry along with our astrometric error ellipse is shown in green. The coordinates of the counterpart in the *F*555*W* + *F*814*W* image are shown as a red cross. The source is relatively blue compared to the surrounding population.

1.3 arcsec). We masked the individual frames in order to remove bad pixels, cosmic rays, and other image artifacts.

Images taken with OSIRIS have known geometric distortions. Therefore, we calculated a distortion correction from observations of the globular cluster M92 observed on 2013 February 13 in K band. These data were reduced using the procedure outlined above, including corrections for flat-fielding using dome flats taken on the same night and in the same configuration. We identified 65 stars common to the Gaia DR1 catalog⁵ and 20 frames of OSIRIS imaging, 15 of which were observed with a position angle (PA) = 0° and 5 of which were observed with PA = 45° . We fit a fifth-order polynomial to the differences Δx and Δy coordinate values resulting from a generalized fit of the OSIRIS imaging to the Gaia DR1 coordinates. From this fit, we calculated a distortion correction for the OSIRIS imager. The standard deviation of the residual offsets of the common sources in the M92 frames was $\sigma_{\alpha} = 0.011$ arcsec and $\sigma_{\delta} = 0.012$ arcsec.

Using these geometric distortion corrections, we resampled the SN 2017ein frames to a corrected grid. Finally, we aligned the individual frames using an offset calculated from the position of the SN and combined them. In Fig. 1, we show the final OSIRIS imaging along with a reference *HST/WFPC2 F814W* image of NGC 3938.

2.3 Photometry

We observed SN 2017ein with SINISTRO g'r' imaging on the 1-m McDonald Observatory Node on the Las Cumbres Global Telescope Network (LCOGTN) from 2017 May 27 to 2017 July 11. These data were reduced using the Obsevatory Reduction and Acquisition Control Data Reduction pipeline (ORAC-DR; Jenness et al. 2015) using estimates of the instrumental bias, dark current, and sky flats obtained on the same night and in the same instrumental configuration. We performed PSF photometry on the final, calibrated frames using sextractor with a PSF constructed empirically from isolated stars in each frame. Using instrumental magnitudes from our PSF-fit photometry, we calibrated our measurements with gr measurements of standard stars from the Pan-STARRS1 (PS1) object catalog (Chambers et al. 2016; Flewelling et al. 2016).

In addition, we observed SN 2017ein with BVr'i' imaging using the Direct CCD on the Nickel 1-m Telescope at Lick Observatory, California. These data were reduced using the photpipe image reduction and photometry package. photpipe is a well-tested and robust pipeline used in several large-scale, optical surveys (e.g. PS1 and SuperMACHO; Rest et al. 2005, 2014). We used photpipe to perform bias-subtraction and flat-fielding then registered the individual images. Finally, we constructed a PSF for each image with DoPhot (Schechter, Mateo & Saha 1993) using isolated stars in the field and then measured instrumental magnitudes for all point sources in the image. The instrumental magnitudes were calibrated using gri magnitudes from stars in the PS1 object catalog with $gri \rightarrow BV$ transformations from Jester et al. (2005).

We also obtained eight epochs of *Swift* Ultraviolet/Optical Telescope (UVOT) imaging of SN 2017ein from the *Swift* data archive. The *HST* images demonstrate that SN 2017ein is close to several clusters and so the structure of the background near the SN is complex. Therefore, we performed PSF photometry on the UVOT imaging using sextractor with instrumental PSF derived from isolated stars in each UVOT image. For images in which we detected SN 2017ein, we derived magnitudes using zero points from the most recent UVOT calibrations. 8

The final photometry from all sources in UBVgri is presented in Table 1 and in Fig. 2.

2.4 Spectroscopy

We observed SN 2017ein over multiple epochs (Table 2) with the Kast double spectrograph on the 3-m Shane telescope at Lick Observatory, California. The 2.0 arcsec slit was used and the 452/3306 grism on the blue side and 300/7500 grating on the red side in conjunction with the d57 dichroic for an approximate effective spectral range of $3\,400-11\,000\,\text{Å}$ and a spectral resolution of $R\approx400\,\text{in}$ each epoch. In each epoch, we aligned the slit to the parallactic angle to minimise the effects of atmospheric dispersion (Filippenko 1982). We performed standard reductions, including bias-subtraction and flat-fielding, on the 2D spectra using pyraf. We extracted the 1D spectra on the blue and red sides using the pyraf task apall. Wavelength calibration was performed on these 1D spectra images

⁵http://gea.esac.esa.int/archive/

⁶https://ziggy.ucolick.org/ckilpatrick/osiris.html

⁷https://swift.gsfc.nasa.gov/archive/

⁸https://heasarc.gsfc.nasa.gov/docs/heasarc/caldb/

Table 1. All UBVgri magnitudes are in the AB system. Uncertainties are given next to each measurement in milli-magnitudes.

Swift/UVOT					
MJD	U	B	V		
57900.51	18.177(130)	_	16.922(069)		
57915.46		16.472(028)	15.305(069)		
57923.03	_	17.056(031)	15.846(036)		
57927.82	18.552(152)	17.457(039)	16.137(040)		
57933.99	18.972(259)	17.768(082)	16.670(050)		
57937.84	19.113(299)		16.759(057)		
57945.28	_	_	16.897(058)		
57949.87	_	18.215(172)	17.109(066)		
57955.39	_	-	17.252(256)		
		Nickel			
MJD	B	V	r	i	
57901.30	17.281(014)	16.613(010)	16.609(010)	16.488(011)	
57902.22	17.094(013)	16.491(009)	16.317(007)	16.371(010)	
57907.25	15.956(008)	15.425(008)	15.506(009)	15.352(009)	
57909.26	15.826(011)	15.237(008)	15.303(008)	15.118(009)	
57930.23	17.552(028)	16.295(018)	15.873(010)	15.401(010)	
57934.24	17.826(038)	16.709(020)	15.992(015)	15.569(013)	
57955.20	18.375(079)	17.169(150)	16.651(011)	_	
57957.20	18.396(076)	17.216(145)	16.702(021)	_	
	LCOGT				
MJD	g	r			
57900.22	_	16.903(018)			
57901.12	16.763(030)	16.620(024)			
57902.12	16.542(024)	16.351(022)			
57914.14	15.488(027)	15.192(016)			
57915.15	15.508(017)	15.201(009)			
57926.19	16.070(024)	15.558(010)			
57935.16	16.804(042)	15.987(020)			
57937.12	16.915(082)	16.319(034)			
57946.14	_	16.580(028)			

using calibration-lamp exposures taken in the same instrumental set-up and configuration. We derived a sensitivity function and performed flux calibration using a standard star spectrum obtained on the same night and in the same setup as our SN 2017ein spectra. Finally, we combined the calibrated 1D spectra using a \sim 100 Å overlap region between the red and blue side spectra. We dereddened each spectrum by E(B-V)=0.018 mag to account for Milky Way reddening and removed the recession velocity of NGC 3938 ($v=809\,\mathrm{km\ s^{-1}}$). The final Kast spectra are presented in Fig. 3.

We also observed SN 2017ein with the Low-Resolution Imaging Spectrograph (LRIS) on the Keck-I telescope on 2017 May 29. We used the 600/4000 grism on the blue side and 400/8500 grating on the red side in conjunction with the D560 dichroic and the 1.0 arcsec long slit, which provides a spectral resolution of $R \approx 700$. SN 2017ein was observed at the parallactic angle at an airmass of \sim 1.47. The LRIS spectrum was reduced using standard techniques and our own IDL routines (as described in Foley et al. 2003). We used a spectrum of the spectrophotometric standard HZ 44 on the blue side and BD+174708 on the red side to flux-calibrate our data and remove telluric lines from the final spectrum. These spectra are shown in Fig. 3.

In addition, we observed SN 2017ein on 2017 June 30 and July 27 with KOSMOS on the KPNO 4-m telescope on Kitt Peak, Arizona. We used the 4-pixel (1.2 arcsec) red slit in a blue set-up with the

B2K Volume Phase Holographic (VPH) grism (3800–6600 Å) and a red set-up with the R2K VPH grism (5800–9400 Å). In this setup, the spectral resolution is $R \approx 700$ on both sides. In the blue and red setups, we used the GG395 and OG530 order-blocking filters, respectively. In both epochs, we integrated for 900 s in the blue and red setups and aligned the slit with the parallactic angle to minimise atmospheric dispersion. We performed similar reductions to the spectra described above, and the final spectra are shown Fig. 3.

Finally, we observed SN 2017ein with the Echellette Spectrograph and Imager (ESI) on the Keck-II telescope on 2017 June 24. We used the 0.5 arcsec slit with ESI and the seeing was around 0.5–0.6 arcsec during observations. We observed in the echellette mode, with a spectral resolution of $R \approx 6000$. These observations were reduced using the ESIRedux IDL package (Prochaska et al. 2003), including bias-subtraction, flat-fielding, and aperture extraction of each order using a boxcar aperture. ESIRedux automatically applies heliocentric and barycentric corrections to the extracted spectra, and so the final spectrum is given in vacuum wavelength. We calibrated each order using a wavelength solution derived from a ArXeHg lamp spectrum observed in the same instrumental configuration. We calculated a sensitivity function for each order using a spectrum of BD+28 4211 observed on the same night and at a similar air-

⁹https://www2.keck.hawaii.edu/inst/esi/ESIRedux

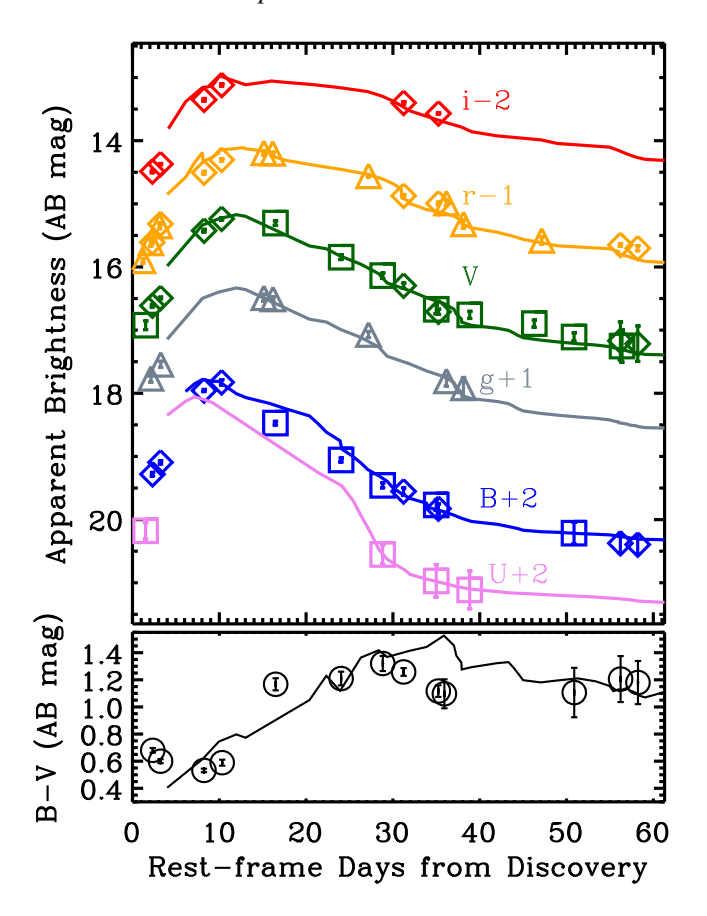


Figure 2. Top: *UBVgri* light curves of SN 2017ein from the LCO Global Telescope Network (triangles), the Nickel telescope (diamonds), and *Swift* (squares). The error bars are given inside of each plotting point. All magnitudes are shown in the AB system with offsets between different bands. For comparison, we overplot *UBVRI* light curves of the carbon-rich SN Ic 2007gr (Bianco et al. 2014) transformed using equations in Jester et al. (2005) into the *UBVgri* system and shifted to match SN 2017ein. Bottom: The B-V colour of SN 2017ein (circles) corrected for Milky Way extinction. We also show the B-V colour of SN 2007gr (black line), which has been shifted by 0.25 mag to match SN 2017ein.

mass to the SN 2017ein spectrum. After flux calibrating each order, we combined the individual orders by taking the inverse-variance weighted average of the overlap region between the orders. The final spectrum is shown in Fig. 3.

3 RESULTS AND DISCUSSION

3.1 Light curves of SN 2017ein

In Fig. 2, we show our full *UBVgri* light curves of SN 2017ein along with comparisons to *UBVRI* light curves of SN 2007gr (Bianco et al. 2014) transformed using equations in Jester et al. (2005) to *UBVgri*. The light curves are all shown in the AB magnitude system and Milky Way extinction has been removed. The comparison SN 2007gr light curves are shifted to match SN 2017ein.

Based on our comparison to SN 2007gr, we determine that SN 2017ein peaked around MJD = 57909.8 \pm 1.2 with an apparent *V*-band magnitude of 15.2 \pm 0.1 mag. Removing Milky Way extinction and at the distance of NGC 3938, this value corresponds to a peak *V*-band absolute magnitude of $M_V = -16.0 \pm 0.2$ mag. Without a significant level of host extinction, this luminosity implies

a relatively faint SN Ic, which typically peak from -17 to -19 mag (Drout et al. 2011; Bianco et al. 2014). Even if SN 2017ein was near the bottom of the SN Ic luminosity function derived in Drout et al. (2011) and identical to SN 2007gr (e.g. with $M_V = -17.2 \pm 0.1$ mag), its host extinction would be at least $A_V = 1.2 \pm 0.2$ mag. With this host extinction, SN 2017ein had a peak V-band luminosity dimmer than 80 per cent of SNe Ic, which have a median V-band peak luminosity of -18.0 mag (Fig. 4). For example, the spectroscopically normal SN Ic 2011bm peaked at around $M_V = -18.5$ mag (Valenti et al. 2012) whereas the SN Ic 2004aw peaked at around -18.1 mag and is closer to the median for SN Ic in terms of V-band magnitude (Taubenberger et al. 2006). Although there is a wide range of diversity in SNe Ic, SN 2017ein and SN 2007gr appear to be at the bottom of the V-band luminosity distribution.

We also compared the host and Milky Way extinction-corrected B-V colour curve of SN 2007gr to the Milky Way extinctioncorrected B - V colour curve of SN 2017ein. The difference in B-V colours is 0.25 ± 0.15 mag on average, although there is some evidence that the evolution in B - V colour for SN 2017ein and SN 2007 gr is different. If we take this difference to be the value of E(B-V) due to extinction in NGC 3938 and assume that the dust is Milky Way-like (i.e, with $R_V = 3.1$), we find that the total host extinction is $A_V = 0.78 \pm 0.47$ mag. However, this host extinction estimate is subject to significant uncertainties, not least the assumption that the overall SN 2017ein light curve is SN 2007gr-like and the totalto-selective extinction ratio R_V . If we assume a high value of R_V = 4.1 then $A_V = 1.0 \pm 0.6$ mag. In other respects, the evolution of the SN 2017ein light curves is typical for SNe Ic. We measure a Δm_{15} in r band of 0.6 ± 0.1 mag, which is nominally smaller but still in agreement with most other SNe Ic including SN 2007gr (e.g. Drout et al. 2011; Bianco et al. 2014).

3.2 Spectra of SN 2017ein

In Fig. 3, we compare our spectra of SN 2017ein to spectra of the SN Ic 2007gr (in gold, from Valenti et al. 2008). The comparison spectra have been de-reddened and their recession velocities have been removed according to the extinction and redshift information in Valenti et al. (2008). For each spectrum, we indicate the epoch relative to the epoch of V-band maximum light. We have also de-reddened SN 2017ein by $A_V = 1.2$ mag to account for host reddening.

At early times, it is evident that the continuum of SN 2017ein is similar to that of SN 2007gr given our choice for reddening in NGC 3938, which again indicates that SN 2017ein has a significant amount of exintction from its host galaxy. Beyond this trend, there is clear overlap between SN 2007gr and SN 2017ein in the level of calcium and, especially, C II λ7235 absorption at early times (Fig. 5). These features fade over time, consistent with a decrease in temperature in the SN photosphere as it expands. However, the similarity in the strength of this feature between SN 2007gr and SN 2017ein is notable, especially as this carbon feature is usually weak or absent in other well-studied SNe Ic (see discussion in Valenti et al. 2008). We also note the presence of C_I around 10400 Å in our day 17 and 27 spectra with a weaker feature in the day -4 spectrum. This evolution is consistent with a decrease in temperature in the SN 2017ein photosphere as the carbon becomes neutral. Beyond these features, SN 2017ein exhibits prominent emission lines of Fe and Ca in its post-maximum spectra. These features are also consistent with SN 2007gr and other SNe Ic as the SN photosphere reveals the inner layers of ejecta.

Table 2. Spectroscopy of SN 2017ein. Phase is indicated in days relative to V-band peak brightness on MJD = 57909.8.

MJD	Phase	Telescope/	Range	R	Grism/ grating	Exposure
		mousileit.	(Å)		5n5	(s)
57902.38	-7	Keck/LRIS	3 120–10 200	700	B600/R400	600
57906.18	-4	Shane/Kast	3 400-10 800	400	B300/R452	1200
57926.28	16	Shane/Kast	3 400-11 000	400	B300/R452	1200
57929.24	19	Keck/ESI	4 051-10 116	6000	Echellette	300
57934.17	24	Mayall/KOSMOS	4 160-10 000	700	B2K/R2K	900/900
57937.23	27	Shane/Kast	3 400-10 800	400	B300/R452	1200
57956.21	46	Shane/Kast	3 400-10 959	400	B300/R452	1200
57961.17	51	Mayall/KOSMOS	4 180–10 000	700	B2K/R2K	900/900

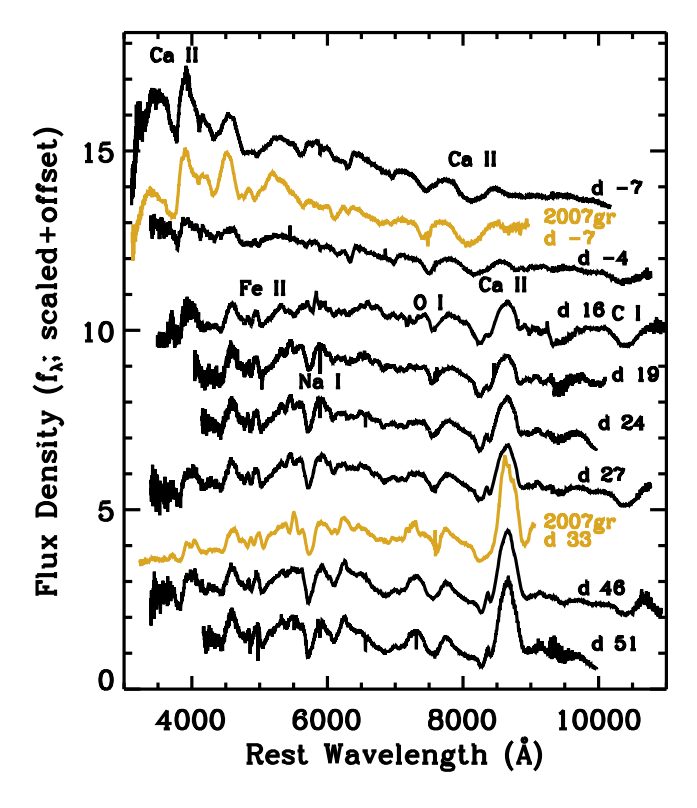


Figure 3. Our full spectral series of SN 2017ein with phase relative to V-band maximum indicated (as in Table 2). The SN 2017ein spectra have been de-reddened assuming $A_V = 1.2$ mag and using the reddening law from Cardelli, Clayton & Mathis (1989) with $R_V = 3.1$. For comparison, we also show two spectra of SN 2007gr from Valenti et al. (2008) in the preand post-maximum phases. Note the prominent carbon bands in both SN 2017ein and SN 2007gr, especially at C II λ 7235.

In Fig. 5, we compare our spectrum of SN 2017ein from \approx 1 week before *V*-band maximum to those of SN 2011bm (which is a spectroscopically 'normal' SN Ic; Valenti et al. 2012) and SN 2007gr (Valenti et al. 2008). These spectra have been de-reddened and their host velocities have been removed, and we de-reddened SN 2017ein by our preferred value of $A_V = 1.2$ mag (discussed below in Section 3.3) such that the continuum matches the comparison spectra. We note the similarity between SN 2007gr and SN 2017ein at this stage, especially in the presence of C II absorption, which is blueshifted in SN 2017ein to a velocity of 12 000 km s⁻¹. We identify C II λ 4267, 6580, and 7235 Å as well as a possible detection of C II λ 3920 Å, although this latter feature is blended with Ca H&K. Valenti et al. (2008) noted the presence of these features in

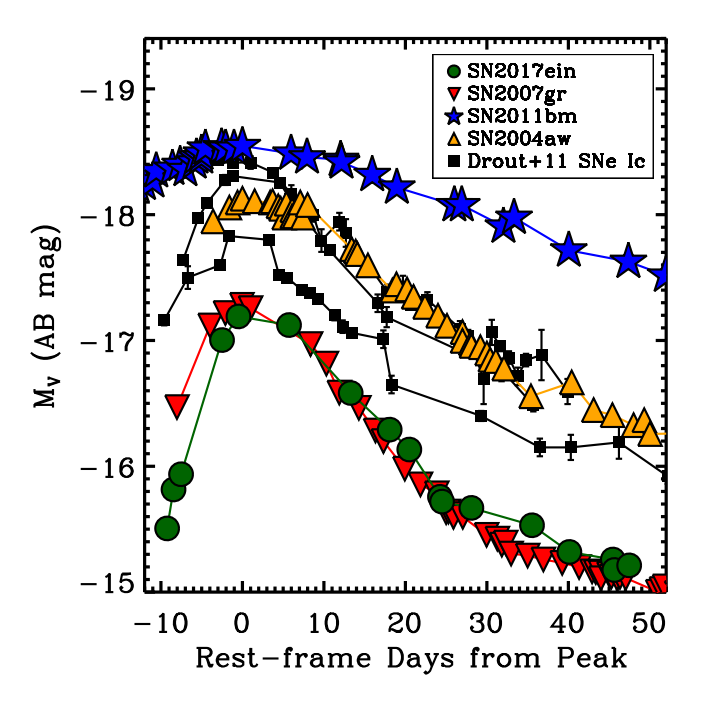


Figure 4. *V*-band light curves of SN 2017ein, SN 2007gr (Bianco et al. 2014), SN 2011bm (Valenti et al. 2012), and SN 2004aw (Taubenberger et al. 2006). We also plot SNe Ic from Drout et al. (2011) (SNe 2004dn, 2005fe, 2005mf) whose light curves are well-constrained near *V*-band maximum light. The error bars on the photometry are smaller than the plotting symbols apart from the Drout et al. (2011) objects, which are shown. These light curves have been de-reddened according to the values given in each reference, and with our preferred host reddening $A_V = 1.2$ mag for SN 2017ein. Note that the peak *V*-band absolute magnitudes of SNe 2017ein and 2007gr are at the bottom of the luminosity function for SNe Ic, which agrees with findings from Drout et al. (2011).

SN 2007gr, and it is clear from Fig. 5 that C $\scriptstyle\rm II$ is relatively strong in SN 2007gr at a similar epoch as SN 2017ein. At the same time, it is clear that the SN Ic 2011bm exhibits little or no evidence for strong carbon absorption, and so SN 2017ein may be relatively carbonrich or else viewed at an angle such that carbon absorption was seen.

Does the presence of these carbon features reflect a high intrinsic carbon abundance or is it simply an effect of the ionizFation state in the ejecta? Mazzali et al. (2010) suggest that the presence of strong carbon features in SN 2007gr reflect a high intrinsic carbon-to-oxygen ratio in the ejecta. However, carbon was still ionized at this epoch indicating that the ejecta were still hot. Therefore, at ≈ 1 week before maximum light, we are only seeing through the

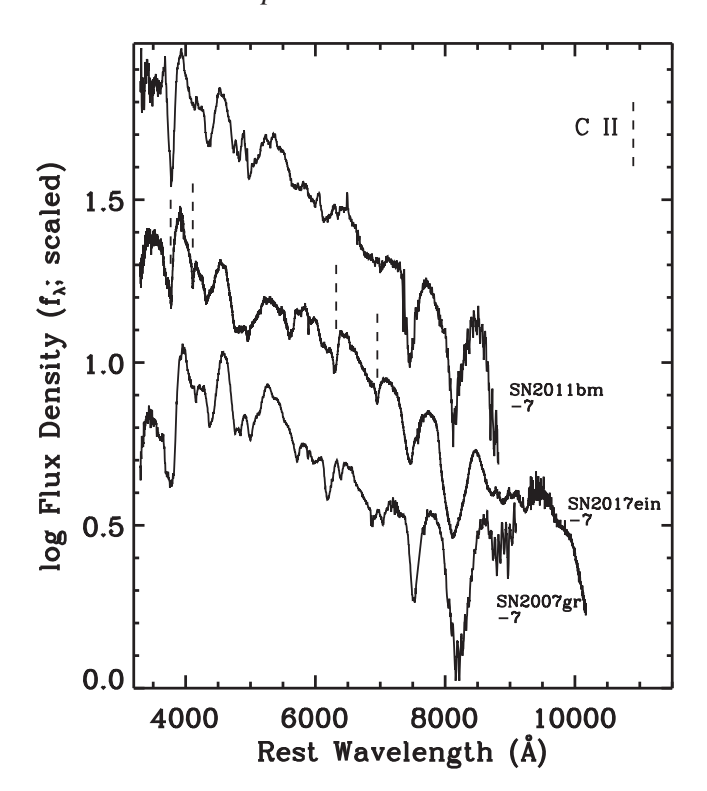


Figure 5. Comparison between our Keck/LRIS spectrum at 7 days before *V*-band maximum to spectra of SN 2011bm (Valenti et al. 2012) and SN 2007gr (Valenti et al. 2008) from 1 week before optical maximum (phase is given in rest days from maximum light). All spectra have been de-reddened and their recessional velocities have been removed according to the values given in each reference. The SN 2017ein spectrum has been de-reddened assuming $A_V = 1.2$ mag and using the reddening law from Cardelli et al. (1989) with $R_V = 3.1$. We mark the presence of C II features in SN 2017ein at 4267, 6580, and 7235 Å as well as a possible detection at 3920 Å. All of these features are blueshifted by $\sim 12\,000\,\mathrm{km}\,\mathrm{s}^{-1}$.

outermost layers of ejecta as most of the SN is still optically thick to electron scattering. Late-time nebular spectra will be critical for evaluating the intrinsic carbon abundance in SN 2017ein and determining whether the similarity to SN 2007gr reflects an intrinsically high carbon abundance.

3.3 Na I D equivalent width and an estimate of the host extinction

In addition to the unusual continuum shape, there is evidence of significant reddening in our spectra in the strong Na_I D features redshifted to the velocity of NGC 3938. These lines are well resolved in our Keck/ESI spectrum (Fig. 6), where we estimate the equivalent width (EW) of the features at the velocity of NGC 3938 to be EW Na_I D₁ = 0.63 \pm 0.01 Å and Na_I D₂ = 0.67 \pm 0.01 Å, for a combined EW of D₁ +D₂ = 1.30 \pm 0.02 Å. Following the relation for Milky Way-like dust in Poznanski, Prochaska & Bloom (2012), we find $E(B-V)=0.47\pm0.05$ mag. We also measure the Na I D EW from Milky Way lines in the ESI spectrum, which is consistent with the reddening value from Schlafly & Finkbeiner (2011).

The NGC 3938 reddening value is significantly larger (at $>1\sigma$) than the value derived by comparing the SN 2017ein and SN 2007gr colour curves. It is possible that this discrepancy reflects an intrinsic difference between the SN 2017ein and SN 2007gr light curves, and

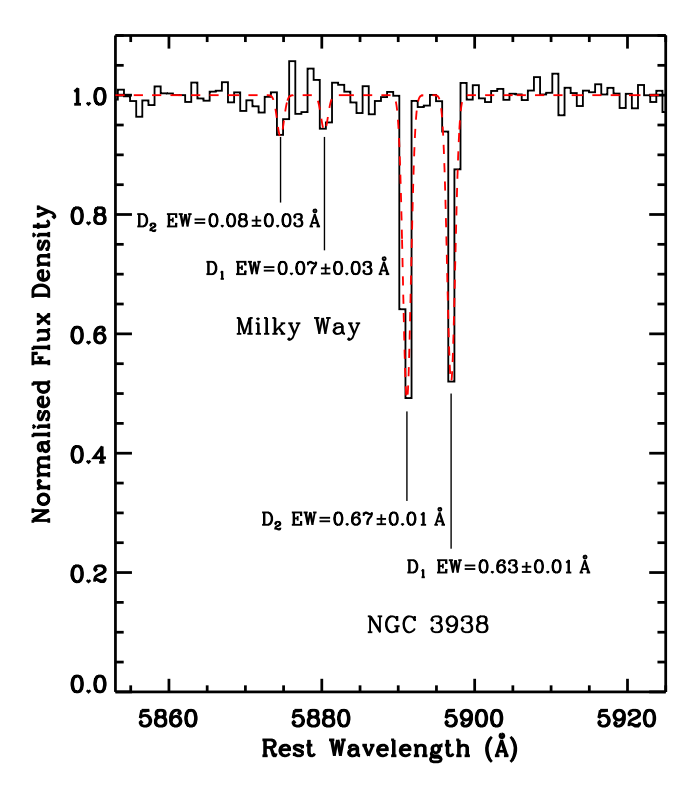


Figure 6. Our normalized Keck/ESI spectrum of SN 2017ein from 20 days after maximum light and centred around the Nai D lines. We detect Nai D at a redshift consistent with both the Milky Way and NGC 3938 and measure the equivalent width in both sets of lines. The Milky Way equivalent width is consistent with the reddening along this line-of-sight as reported in Schlafly & Finkbeiner (2011). As we discuss in Section 3.2, the NGC 3938 equivalent width is consistent with a very high host extinction, from $A_V = 1.2-1.9$ mag depending on the total-to-selective extinction ratio.

so our comparison between these objects is flawed. In this case, Nat D provides a more reliable estimate of the total host extinction to SN 2017ein, although converting the value of E(B-V) to an in-band extinction involves further assumptions about the host extinction properties.

Variation in dust properties in SN host galaxies is a major uncertainty, and some examples are known to have dust unlike the Milky Way (e.g. SN 2014J in M82; Gao et al. 2015). For a reasonable range of total-to-selective extinction ratios (e.g. $R_V = 2.5 - 4.1$), the reddening we derive from Na I D could imply a host extinction to SN 2017ein from $A_V = 1.2-1.9$ mag.

SN 2017ein is similar to the relatively low-luminosity SN Ic 2007gr, and although the intrinsic B- and V-band magnitudes and colour curves of these objects may be discrepant (at the 0.2 mag level), the V-band host extinction to SN 2017ein implied by this comparison is 1.2 ± 0.2 mag. This extinction value implies $R_V = 2.6$ assuming $E(B-V) = 0.47 \pm 0.05$ mag from Na I D. We adopt this value for the 'preferred' extinction to the SN 2017ein progenitor system in our subsequent analysis, although there are still large uncertainties on this estimate. A_V could be 0.7 mag larger than this value for $R_V = 4.1$, but this value would be inconsistent with our fits to the SN 2007gr V-band light curve and B-V colour curves, which are both consistent with lower values close to $A_V \approx 1.2$ mag. Therefore, while we use this value throughout the rest of the paper, the total systematic uncertainty on the host extinction is large. Reasonable estimates on the value of

 A_V range from roughly 1.2 mag (implying $R_V = 2.5$) to 1.9 mag ($R_V = 4.1$).

All extinction estimates from the SN neglect the possibility of circumstellar dust that affected the progenitor observables but was destroyed by the SN. We do not see evidence for excess emission in the early-time light curve or spectroscopy of SN 2017ein that would be consistent with interaction between the SN shock and a significant mass of dust (as in SNe IIn, e.g. Fox et al. 2011; Kilpatrick et al. 2018). Considering that SN 2017ein may have been discovered very soon after explosion (as suggested by Im et al. 2017), we predict that we would have observed excess emission from a large mass of dust, and so we find the presence of such dust to be unlikely.

3.4 Relative astrometry between the adaptive optics and *HST* imaging

We performed relative astrometry between the OSIRIS image and composite *HST* image using the 18 common sources circled in both frames (Fig. 1). The positions derived for these 18 sources were determined using dolphot in the *HST* frame and sextractor in the OSIRIS frame. We performed image registration on the LGSAO image using the IRAF tasks ccmap and ccsetwcs. We used default parameters for ccmap, which fit pixel coordinates from the stars identified in our LGSAO imaging to a tangent plane projection of the right ascensions and declinations of the same stars in the *HST* image. We used a general geometric fit, which included terms for linear shift, rotation, and the relative pixel scale between the images.

We estimated the astrometric uncertainty of our best-fitting geometric projection by randomly sampling half of the common sources and calculating a geometric solution then calculating the average offset between the remaining common sources in this projection. On average, we found $\sigma_{\alpha} = 0.040$ arcsec and $\sigma_{\delta} = 0.037$ arcsec. Within the combined uncertainties (totalling $\sigma_{\alpha} = 0.041$ arcsec and $\sigma_{\delta} = 0.039$ arcsec) of the relative astrometry, the position of SN 2017ein in our LGSAO image, and the geometric distortion correction, we find a single source at the location of SN 2017ein in the reference HST image, which we call S1 (Fig. 1). S1 is located at $\alpha = 11^{\rm h}52^{\rm m}53^{\rm s}.264$, $\delta = +44^{\circ}07^{'}26''.619$ and is detected in the combined HST frame with S/N = 46 for an astrometric precision of 0.004 arcsec. This is also the same source that Van Dyk et al. (2018) identify as the counterpart to SN 2017ein. As we demonstrate in Fig. 1, S1 is offset from the position of SN 2017ein as determined from our LGSAO image by 0.037 arcsec, or approximately 0.75σ . In the HST image, we do not detect any other sources within a 0.343 arcsec (8.6σ) radius of the position of SN 2017ein. Therefore, we consider S1 to be the only viable candidate as the counterpart to SN 2017ein.

We estimate the probability of a chance coincidence in the *HST* image by noting that there are a total of 102 sources (including extended sources) with S/N > 3 within a 10 arcsec radius of SN 2017ein in the *HST* image from Fig. 1. Therefore, the fraction of the total solid angle within 10 arcsec of SN 2017ein that is within 3σ of a detected source is approximately $102 \times (3 \times 0.04 \, \text{arcsec}/10 \, \text{arcsec})^2 = 1.5 \, \text{per cent}$. This value represents the probability that the detected point source is a chance coincidence. Therefore, although it is unlikely that the identified point source is a chance coincidence, there is some probability that this is the case. Follow-up imaging will be critical in order to confirm or rule out this possibility.

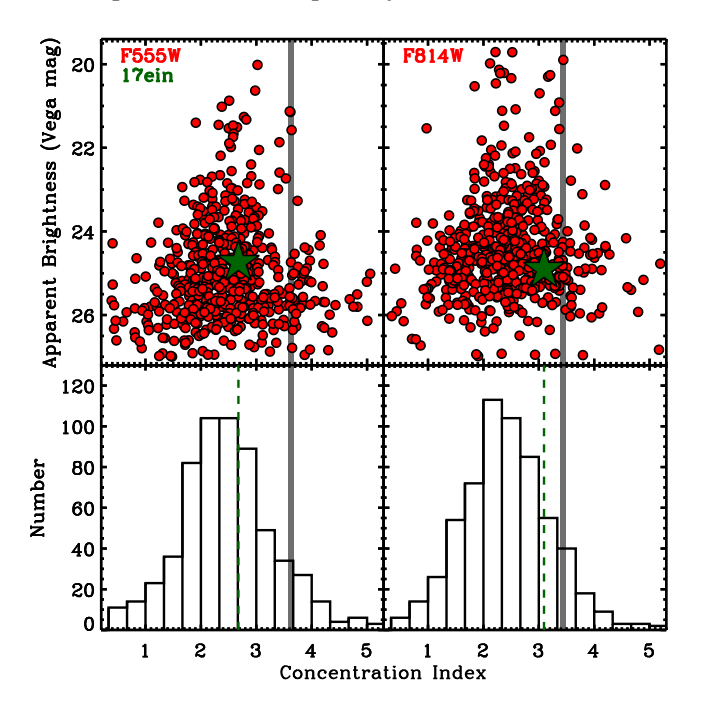


Figure 7. Top left: Concentration index versus Vega magnitude for sources in the HST/WFPC2 F555W images of NGC 3938. The value for the S1 counterpart to SN 2017ein (Section 3.4) is shown as a green star. The shaded region shows the nominal split between clusters and stars at a concentration index of 3.63 in F555W as discussed in Section 3.5.1. Top right: Same as the top left but for the F814W image with the concentration index threshold set at 3.44. Bottom left: A histogram of the F555W values shown in the upper left plot as a function of concentration index. The value for S1 is shown as greek dashed lines. Bottom right: Same as the bottom left but for the F814W values

3.5 Photometry and classification of the pre-explosion counterpart

3.5.1 HST photometry and the PSF of the pre-explosion counterpart

From our photometric analysis of S1, we obtained Vega magnitudes $m_{F555W} = 24.787 \pm 0.041$ mag and $m_{F814W} = 24.902 \pm 0.075$ mag. These values are nominally fainter than those found in Van Dyk et al. (2018), who report $m_{F555W} = 24.56 \pm 0.11$ mag and $m_{F814W} = 24.58 \pm 0.17$ mag. These differences originate from the different dolphot parameters used in fitting, ¹⁰ which we adjusted to fit for the complex local background around S1.

Photometry from the combined F555W + F814W imaging suggests that the object at the position of SN 2017ein has sharpness =-0.061 and roundness =0.053, which is generally consistent with a single point source. However, the PSF of the source in both F555W and F814W is somewhat extended and eccentric, with PSF eccentricities 0.221 and 0.218, respectively. The source may be partially contaminated by emission from a nearby cluster (it has dolphot crowding parameter 0.163; see Fig. 1), hence our use of a local background estimate in performing photometry (Section 2.1), although it is possible that this background emission somewhat affects the PSF parameter estimates.

We further investigated the possibility that S1 is an extended source by measuring a 'concentration index' (Fig. 7). Following analysis in Chandar et al. (2010) for *HST/WFC3* photometry, we

 $^{^{10}}$ Van Dyk et al. (2018) use FitSky=3 and img_RAper=8.

calculated the difference in magnitudes for a circular aperture with radius 0.5 pixels and an aperture with radius 3.0 pixels centred on the PSF-fit coordinates and using the same local background estimate from dolphot. We restricted our analysis to sources within 10 arcsec of SN 2017ein, and so all of the sources we investigated landed on the same WF2 array as SN 2017ein.

We found a concentration index of 2.677 in F555W and 3.094 in F814W. Larger concentration indices imply that most of the emission of the source is spread out at large separations from the centre of the PSF. Chandar et al. (2010) define a threshold concentration index for distinguishing between stars and clusters by examining candidate objects that are thought to be stars or clusters and finding the maximum and minimum concentration indices of these distributions. These thresholds cleanly separate sources detected using WFC3 into distributions of stars and clusters (see e.g. Fig. 4 in Chandar et al. 2010). We estimate a similar threshold by examining the concentration index below which we find 95 per cent of objects with m < 25 mag, which are more likely to be clusters. This value is 3.63 for F555W and 3.44 for F814W. In both cases, the SN 2017ein candidate lies within the distribution and could reasonably be considered to be a single, unresolved point source. However, in F814W, the source is much closer to the limit we have defined, which is relatively crude compared to the analysis in Chandar et al. (2010).

If S1 is a cluster, then it is extremely young. The $m_{F555W} - m_{F814W}$ (roughly V-I) colour corrected for Milky Way extinction and assuming no host extinction is -0.143 mag, which is consistent with a 4 Myr cluster (Bruzual & Charlot 2003; Peacock, Zepf & Finzell 2013). With added host extinction, the source would be even bluer and younger, implying that any star that exploded from the population in this cluster had an initial mass $>73M_{\odot}$ for a single star (as derived from MIST evolutionary tracks; Choi et al. 2016).

If S1 is a marginally unresolved cluster, then only the most extreme and massive single star populations could explain the colours for this source. At 4 Myr, these sources would have $M_V < -10$ mag or an unabsorbed magnitude of $m_{F555W} \approx 21.2$ mag at the distance of NGC 3938. Unless the host extinction is $A_V > 4$ mag to SN 2017ein, it is unlikely that S1 is such a star. We find that the most likely scenario is a luminous, blue source corresponding to a single star or multiple star system with a surrounding population of less luminous sources. These other sources are likely unresolved stars still on the main sequence. This scenario agrees with the magnitudes, colours, and concentration for S1.

If the full dolphot photometry for S1 is partly contaminated by a surrounding population of stars, we can remove some of this light using forced photometry. We used the instrumental PSFs for HST/WFPC2 in F555W and F814W to fit photometry to S1 and found that the central source was marginally fainter without the extended emission: the PSF-fit source, which we call PSF1 had brightnesses $m_{F555W} = 24.901 \pm 0.062$ and $m_{F814W} = 25.112 \pm 0.121$. If a single object dominates the emission from this source and is the pre-explosion counterpart to SN 2017ein, then these magnitudes represent its total emission. Otherwise, if one or more unresolved sources contributes significantly to the emission within the PSF, then these magnitudes are only upper limits on the pre-explosion emission from the SN 2017ein progenitor star.

3.5.2 Classification of the pre-explosion counterpart

We corrected the *HST* photometry of PSF1 for interstellar extinction using the extinction law in Cardelli et al. (1989) with $A_V = 0.058$

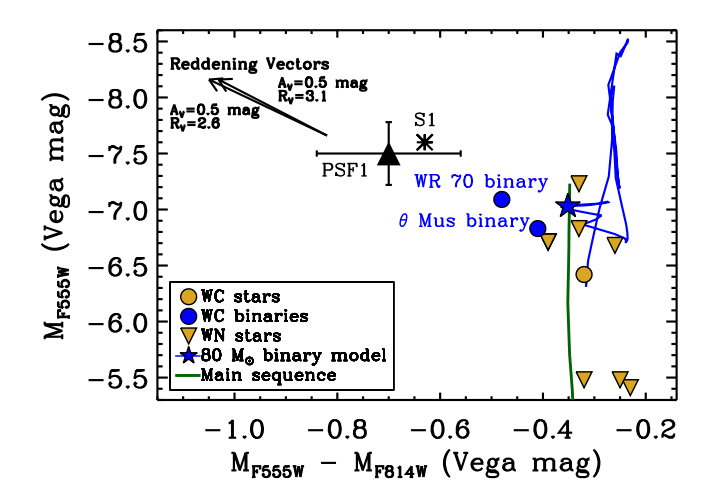


Figure 8. Colour-magnitude diagram showing the properties of the forced photometry from the SN 2017ein pre-explosion counterpart (PSF1). The values for F555W luminosity, and F555W – F814W colour are described in Section 3.5.2. We have corrected for our preferred host reddening of $A_V = 1.2$ mag. The uncertainties are based on the photometry and distance modulus. We also indicate reddening vectors corresponding to $A_V = 0.5$ mag with $R_V = 2.5$ and 4.1. For comparison, we show the full photometry, including extended emission around the source S1. We also plot a MIST model for the zero age main sequence for a population of stars at the metallicity of NGC 3938 (green line) as well as a BPASS model for an 80+48M_O binary with initial period P = 10 days (blue line). The terminal state of the BPASS model is shown with a blue star. Several Galactic WR systems are shown as orange triangles (WN stars) and orange circles (WC stars). All of these WR stars represent the emission from the WR star itself apart from the WC9+B star binary WR 70 and the WC6+O binary θ Mus (blue circles; labelled), which are dominated by the spectral energy distributions of their companion

and $R_V = 3.1$ and host extinction using $A_V = 1.2$ mag with $R_V = 2.6$ (implying $A_I = 0.6$ mag) as discussed in Section 3.3. Assuming $m - M = 31.17 \pm 0.10$, PSF1 had luminosities $M_{F555W} = -7.5 \pm 0.2$ mag (roughly V band) and $M_{F814W} = -6.7 \pm 0.2$ mag (roughly I band). We plot these values in Fig. 8 along with the corresponding values for S1. Clearly the added light from extended emission does not make a significant difference to the final photometry of PSF1 relative to the uncertainties.

The extinction-corrected F555W-F814W colour is -0.67 ± 0.14 mag (with systematic uncertainties represented by variations in reddening; Fig. 8). This colour is blueward of the main sequence and implies a much hotter star than the vast majority of stars. For example, the bluest V-I colour for a star in the *Hipparcos* and Tycho2 catalogue is V-I=-0.49, although this estimate is subject to significant selection bias due to Galactic dust. At the very least, this colour implies a spectral energy distribution that peaks far blueward of V band and a source with a very hot photosphere. Some late-type WN stars (also WNL; Wolf-Rayet stars with low-ionization state nitrogen lines in their spectra; Hamann, Gräfener & Liermann 2006; Crowther 2007a; Sander, Hamann & Todt 2012) are luminous enough to match the properties of PSF1 with $M_V = -7.6$ mag, but typically only have V-I colours as blue as -0.3 mag.

If we assume the source with $M_{F555W} = -7.5 \pm 0.2$ mag and F555W - F814W colour -0.67 ± 0.14 mag is dominated by a single star, then by comparison to MIST models (Paxton et al.

2011, 2013, 2015; Choi et al. 2016; Dotter 2016),¹¹ we find that the best-fitting bolometric correction for such a star is $BC_{F555W} = -2.8 \pm 0.4$ mag. The best-fitting luminosity for a single star at the metallicity of NGC 3938 [log $(O/H) = 8.94 \pm 0.05$; Kudritzki et al. 2015] is approximately log $(L/L_{\odot}) = 6.0 \pm 0.2$, implying an initial mass of $55^{+20}_{-15} \rm M_{\odot}$.

The evolutionary pathway such a high-mass star would take to end as a highly stripped SN Ic progenitor is less certain. It has been hypothesized that WC stars (WR stars with strong carbon emission lines in their spectra; Crowther 2007a) are likely candidates for SNe Ic (Dessart, Livne & Waldman 2010; Dessart et al. 2012; Yoon et al. 2012; Dessart et al. 2015; Yoon 2015b). The Galactic population of WC stars generally have absolute magnitudes $M_V = -3$ to -5.5 mag with V - I colours bluer than WNL stars (van der Hucht 2001; Crowther 2007b). Most SN Ic progenitor star models propose that the final mass ought to be very low in order to explain the observed abundances of SNe Ic, with $17M_{\odot}$ at the most (Meynet & Maeder 2003; Yoon 2015b).

We examined Galactic WR stars with detailed photometry, extinction, and distance estimates (from the VIIth catalogue of Galactic WR stars; van der Hucht 2001) to determine whether any known stars are luminous and blue enough to match PSF1. We restricted our sample to stars without detected companions so we could examine the intrinsic colours and luminosities of WR stars. None of the stars in our sample had colours and luminosities that matched PSF1, and only a few WN stars had luminosities or colours that approached PSF1 (examples with the most luminous M_V magnitudes and bluest V - I colours are shown in Fig. 8).

However, roughly 40 per cent of Galactic WR stars are in binaries, often where the WR star itself does not dominate the overall spectral energy distribution. There are some examples of WR stars in binaries with O- or B-type supergiants that could agree with the luminosity and colours of PSF1. All known examples in the VIIth catalogue of Galactic WR stars with $M_V < -6.5$ mag and V - I <-0.3 mag are late-type WC stars with O- or B-type supergiant companion stars. For example, the WC9 star WR 70 (also HD 137603; Williams & van der Hucht 2000) is in a binary with a B0I supergiant with intrinsic $M_V = -7.09$ mag and V - I = -0.48 mag while the W6+O binary θ Mus has $M_V = -6.83$ mag and V - I = -0.41 mag (Moffat & Seggewiss 1977; Stupar, Parker & Filipović 2010). Both of these stars could match the observed colours and luminosity of PSF1 if we decreased the amount of reddening closer to the lower limit of the range allowed by spectroscopy and photometry of SN $2017ein (A_V = 0.5 mag).$

If PSF1 is dominated by light from a star other than the progenitor star of SN 2017ein, it could simply be in the same cluster as SN 2017ein. The precision of our astrometry indicates that there could be as much as a 0.03 arcsec offset between SN 2017ein and the transient source we identified in pre-explosion imaging, corresponding to ~3 pc at the distance to NGC 3938. If the stars were 3 pc away from the SN 2017ein progenitor star, it would be unassociated with the progenitor system. On the other hand, if PSF1 is dominated by the progenitor system of SN 2017ein and the actual progenitor star is the less luminous component of a binary system, then the two components should be coeval and the luminosity and colour of the more luminous source can be used to constrain the properties of the other component.

Therefore, we analysed all Binary Population and Stellar Synthesis (BPASS2.1; Eldridge et al. 2017) models to look for binary

star models that terminate with a total luminosity $M_V < -7.0$ mag and colour V - I < -0.35 mag. We restricted our search to models with the metallicity of NGC 3938, but otherwise searched the entire range of models with primary initial mass 0.1–300M_☉, initial mass ratio 0.1-0.9, and initial log period (days) 0-4, consisting of 12 664 models. There were two such models in the overall sample that terminated within the selected parameter space, both with primary mass 80M_{\top}. These two models, which we will call Models 1 and 2, have initial mass ratios 0.6 and 0.8 and log periods 1 and 0.8, respectively. Models 1 and 2 end with the secondary star comprising \sim 80 per cent of the overall V-band luminosity, although in both cases this star is somewhat redder $(V - I \approx -0.27 \text{ to } -0.31$ mag) than the overall system. The final mass of the primary star in Model 1 (wider/smaller initial mass ratio) is 15.4M_☉ while in Model 2 (closer/larger initial mass ratio) the primary terminates with $52.2M_{\odot}$.

If the host reddening to SN 2017ein was relatively low ($A_V = 0.7$ mag), then the colour and luminosity of PSF1 could agree with Model 1 (shown in blue in Fig. 8). In addition, Model 1 terminates with effectively no hydrogen and only $0.20 M_{\odot}$ of helium. The total helium mass fraction in the star is quite low (<0.1), and even for a relatively low total ejecta mass, the helium mass fraction in the ejecta would be consistent with predictions for SN Ic progenitor stars (which suggest that a mass fraction <0.5 is sufficient to hide helium lines Dessart et al. 2011; Yoon 2015a).

The luminosity and colour of Model 1 are somewhat similar to WC+O star binaries, where the primary has undergone significant stripping and/or radiative mass loss and ends up as a relatively low mass star. The fact that the primary star in this model has a somewhat high mass for a WC star (which typically range from 4 to 9M_☉; for a review see Crowther 2007b) could be explained by the WR mass-loss prescription or a slightly higher metallicity at the location of SN 2017ein in NGC 3938. Alternatively, this type of binary could simply be a rare system with a high-mass WC star that explodes promptly. Ultimately, the full implications for the initial metallicity, mass-loss prescription, and binary parameters of this system are complex, and additional modelling is needed to explore WC star binaries as potential SN Ic progenitor stars.

4 THE NATURE OF SN 2017EIN AND ITS PROGENITOR SYSTEM

We find a luminous, blue source (S1) at the progenitor site of SN 2017ein. The environment around S1 is consistent with the environments of SNe Ic as a whole; these SNe preferentially explode in regions of high star formation rates (Galbany et al. 2014, 2016), which strongly suggest a high mass (>25 $\rm M_{\odot}$) progenitor star that evolves and explodes close to the region where it formed. However, the diversity of SNe Ic as a whole, and in particular their progenitor systems, is still poorly understood. It is possible that SN 2017ein is atypical for SNe Ic, implying an unusual progenitor system.

From our analysis of the pre-explosion photometry, S1 appears marginally extended, and may be consistent with a massive star cluster. Indeed, it has been found that many stripped-envelope SNe are discovered in or near such clusters (Fremling et al. 2016; Maund 2018). The fact that S1 is more extended in the redder F814W band suggests that the surrounding population of unresolved sources come from stars with lower mass than the star or stars dominating S1. If we assume that S1 is dominated by emission from a single star, then it has a best-fitting mass of $55^{+20}_{-15} M_{\odot}$. This mass range is consistent with the findings of Van Dyk et al. (2018), who report the source is consistent with a star with an initial mass of 60– $80M_{\odot}$ at

¹¹http://waps.cfa.harvard.edu/MIST/

the most for binary star models, or in the range of $47\text{--}48\mathrm{M}_{\odot}$ for single star models.

SN 2017ein could have exploded from a star in a multiple system where the primary does not dominate the overall spectral energy distribution. Late-type WC stars often occur in systems with O- or B-type supergiant companion stars, such as the WC9+B binary WR 70 or the WC6+O star binary θ Mus (Fig. 8). Many of these systems lack detailed orbital parameters, and so it is difficult to place strong constraints on the nature of the WC star itself. WR 70 is a relatively high-mass WC star (9.8M_O Nugis & Lamers 2002) and, as a latetype WC star, likely has an intrinsically high carbon abundance (Smith & Willis 1982). The overall luminosity is dominated by the B-type supergiant companion star, and so the total luminosity of this particular system is a poor indicator of the mass of the WC star. Comparison to binary star models suggests it may be possible to obtain such a system with an $80+48 M_{\odot}$ system, although the mass of the final component is somewhat large. However, this system is left with 0.2M_☉ of helium, which agrees with progenitor model predictions for SNe Ic (Dessart et al. 2011; Yoon 2015a). If the SN 2017ein progenitor star evolved in a similar system with the luminosity and colours observed from PSF1, then it could still be relatively low mass, although the exact mass of the progenitor system and its overall abundances are still highly uncertainty.

From the light curve and spectra of SN 2017ein, we infer that this source is most similar to carbon-rich, low-luminosity SNe Ic such as SN 2007gr as opposed to other SNe Ic such as SN 2011bm. This finding underscores the fact that the SN 2017ein progenitor star must have been hydrogen- and helium-deficient, but could also be relatively carbon-rich. Mazzali et al. (2010) and Valenti et al. (2008) noted that the presence of strong carbon features at early times in SN 2007gr was consistent with an intrinsically high carbon-to-oxygen ratio in the progenitor star.

Our preferred maximum V-band absolute magnitude, assuming a host extinction of $A_V = 1.2$ mag, suggests that SN 2017ein peaked at $M_V = -17.2 \pm 0.2$ mag. This value is at the lower end of the luminosity function for SNe Ic as a whole (Drout et al. 2011), and is consistent with a relatively low mass of 56 Ni ($<0.1 M_{\odot}$), also similar to SN 2007gr. Mazzali et al. (2010) point out that such a low 56 Ni mass implies the explosion of a relatively low-mass CO core; in the case of SN 2007gr, this core likely resulted from a star with a main-sequence mass of $\sim 15 M_{\odot}$ and a relatively low terminal mass (see also Kim, Yoon & Koo 2015). Yoon et al. (2010) suggest that these systems result from stars with a relatively low initial mass ($<25 M_{\odot}$) in order to explain the lack of helium and range of nickel masses.

This is in conflict with the $80+48M_{\odot}$ binary model that provided the best match to the parameters of PSF1, where the 80M_☉ star terminated at $15.4 M_{\odot}$. It is possible that this is a result of systematic uncertainties in the models themselves. Only 2 out of 12 664 BPASS models approached the properties of PSF1, whose extreme colour and magnitude imply a massive, O- or B-type star. Stars in this region of colour-magnitude diagrams are not usually expected to explode, and so the lack of models that terminate here may reflect a physical limitation as much as systematic uncertainties in model parameters. On the other hand, Yoon (2015a) point out that in binary progenitor models for SNe Ib/c, the terminal mass of the primary star is quite sensitive to the choice of metallicity, mass-loss, and masstransfer prescriptions. It is theoretically plausible that extreme mass transfer could produce a low terminal mass from an 80M_O star (see e.g. fig. 10 in Yoon 2015a). However, such a scenario must be verified with late-time imaging to look for variations in the colour and magnitude of the pre-explosion source.

5 CONCLUSIONS

We present pre-explosion imaging and high-resolution imaging, photometry, and spectroscopy of the SN Ic 2017ein. We find:

- (i) Spectra and light curves of SN 2017ein are remarkably similar to carbon-rich, low-luminosity SNe Ic such as SN 2007gr and unlike SNe Ic such as 2011bm. At the same time, matching the continuum and peak V-band luminosity of SN 2017ein to SN 2007gr requires roughly $A_V=1.2\,$ mag of host extinction. We also detect strong Na 1 D absorption at the approximate redshift of NGC 3938. These spectral characteristics suggest that the progenitor system contained very little hydrogen or helium, but also that it may have had an intrinsically high carbon abundance in its outer layers, as has been suggested for some WC stars.
- (ii) The location of SN 2017ein as determined from highresolution laser guide star adaptive optics imaging is consistent with a single source in pre-explosion *HST/WFPC2* imaging. The source is marginally extended in the *HST/WFPC2* images and there may be non-uniform background emission at this location.
- (iii) Accounting for the extended source and host extinction, photometry from the pre-explosion is consistent with single stars with masses up to $75M_{\odot}$, but with a preferred mass of $55M_{\odot}$. However, most of these stars, which include O- and B-type supergiants and WN stars, are hydrogen-rich, and so are unlikely SN Ic progenitor stars
- (iv) Comparison to highly stripped WR star binaries indicates that the only systems that match the colours and luminosity of PSF1 are WC+O and B star binaries. We find that an $80\text{+}48\mathrm{M}_{\odot}$ BPASS model can explain some of the parameters of SN 2017ein and the pre-explosion counterpart and produces a star whose terminal state is roughly consistent with predictions of SN Ic progenitor stars. Additional modelling is needed to explore the full ramifications of this evolutionary pathway and the precise terminal state of such a system.
- (v) Nebular spectroscopy of SN 2017ein will be critical for measuring the true carbon abundance in the ejecta. Late-time imaging of the site of SN 2017ein will also be important for measuring the extent to which the SN 2017ein progenitor star contributed to emission from the pre-explosion source.

ACKNOWLEDGEMENTS

We thank Raj Chowdhury and Bella Nguyen for help with Nickel observations. We also thank David Coulter, César Rojas-Bravo, and Matthew Siebert for help with Shane and Mayall observations.

The UCSC group is supported in part by NSF grant AST-1518052, the Gordon & Betty Moore Foundation, the Heising-Simons Foundation, and by fellowships from the Alfred P. Sloan Foundation and the David and Lucile Packard Foundation to RJF.

Some of the data presented herein were obtained at the W. M. Keck Observatory, which is operated as a scientific partnership among the California Institute of Technology, the University of California, and NASA. The observatory was made possible by the generous financial support of the W. M. Keck Foundation. We wish to recognise and acknowledge the cultural significance that the summit of Mauna Kea has within the indigenous Hawaiian community. We are most fortunate to have the opportunity to conduct observations from this mountain.

Some of the data in this publication were calibrated using object catalogues from the Pan-STARRS1 Surveys. The Pan-STARRS1 Surveys (PS1) and the PS1 public science archive have been made possible through contributions by the Institute for Astronomy, the

University of Hawaii, the Pan-STARRS Project Office, the Max-Planck Society and its participating institutes, the Max Planck Institute for Astronomy, Heidelberg and the Max Planck Institute for Extraterrestrial Physics, Garching, The Johns Hopkins University, Durham University, the University of Edinburgh, the Queen's University Belfast, the Harvard-Smithsonian Center for Astrophysics, the Las Cumbres Observatory Global Telescope Network Incorporated, the National Central University of Taiwan, the Space Telescope Science Institute, the National Aeronautics and Space Administration under Grant No. NNX08AR22G issued through the Planetary Science Division of the NASA Science Mission Directorate, the National Science Foundation grant no. AST-1238877, the University of Maryland, Eotvos Lorand University (ELTE), the Los Alamos National Laboratory, and the Gordon and Betty Moore Foundation.

The Hubble Space Telescope (HST) is operated by NASA/ESA. The HST data used in this manuscript come from programme GO-10877 (PI Li). Some of our analysis is based on data obtained from the HST archive operated by STScI.

We acknowledge the use of public data from the Swift data archive.

Some of the data presented in this manuscript come from the Kitt Peak National Observatory (KPNO) 4-m telescope through programme 2017A-0306 (PI Foley). KPNO is operated by the Association of Universities for Research in Astronomy, Inc. (AURA) under cooperative agreement with the National Science Foundation.

The Nickel and Shane telescopes are operated by the University of California and Lick Observatories. Some of the data presented in this manuscript come from UCO/Lick programmes 2017Q2-N007, 2017Q3-N005 (PI Kilpatrick) and 2017A-S011, 2017B-S018 (PI

This work makes use of observations performed by the Las Cumbres Global Telescope Network through programme 2017AB-012 (PI Kilpatrick).

Facilities: Keck (ESI/LRIS/OSIRIS), LCOGTN (SINISTRO). Mayall (KOSMOS), Nickel (Direct), Shane (Kast), Swift (UVOT)

REFERENCES

Aldering G., Humphreys R. M., Richmond M., 1994, AJ, 107, 662 Arbour R., 2017, Transient Name Server Discovery Rep., 588 Bianco F. B. et al., 2014, ApJS, 213, 19 Bruzual G., Charlot S., 2003, MNRAS, 344, 1000

Cao Y. et al., 2013, ApJ, 775, L7

Cardelli J. A., Clayton G. C., Mathis J. S., 1989, ApJ, 345, 245

Chambers K. C. et al., 2016, preprint (arXiv:1612.05560)

Chandar R. et al., 2010, ApJ, 719, 966

Choi J., Dotter A., Conroy C., Cantiello M., Paxton B., Johnson B. D., 2016, ApJ, 823, 102

Crockett R. M. et al., 2007, MNRAS, 381, 835

Crockett R. M. et al., 2008, MNRAS, 391, L5

Crowther P. A., 2007a, ARA&A, 45, 177

Crowther P. A., 2007b, ARA&A, 45, 177

Dessart L., Livne E., Waldman R., 2010, MNRAS, 405, 2113

Dessart L., Hillier D. J., Livne E., Yoon S.-C., Woosley S., Waldman R., Langer N., 2011, MNRAS, 414, 2985

Dessart L., Hillier D. J., Li C., Woosley S., 2012, MNRAS, 424, 2139

Dessart L., Hillier D. J., Woosley S., Livne E., Waldman R., Yoon S.-C., Langer N., 2015, MNRAS, 453, 2189

Dotter A., 2016, ApJS, 222, 8

Drout M. R. et al., 2011, ApJ, 741, 97

Eldridge J. J., Fraser M., Smartt S. J., Maund J. R., Crockett R. M., 2013, MNRAS, 436, 774

Eldridge J. J., Stanway E. R., Xiao L., McClelland L. A. S., Taylor G., Ng M., Greis S. M. L., Bray J. C., 2017, PASA, 34, e058

Filippenko A. V., 1982, PASP, 94, 715

Flewelling H. A. et al., 2016, preprint (arXiv:1612.05243)

Foley R. J. et al., 2003, PASP, 115, 1220

Fox O. D. et al., 2011, ApJ, 741, 7

Fremling C. et al., 2016, A&A, 593, A68

Gal-Yam A. et al., 2005, ApJ, 630, L29

Gal-Yam A. et al., 2007, ApJ, 656, 372

Galbany L. et al., 2014, A&A, 572, A38

Galbany L. et al., 2016, MNRAS, 455, 4087

Galbany L. et al., 2017, MNRAS, 468, 628

Gao J., Jiang B. W., Li A., Li J., Wang X., 2015, ApJ, 807, L26

Hainich R., Pasemann D., Todt H., Shenar T., Sander A., Hamann W.-R., 2015, A&A, 581, A21

Hamann W.-R., Koesterke L., Wessolowski U., 1995, A&A, 299, 151

Hamann W.-R., Gräfener G., Liermann A., 2006, A&A, 457, 1015

Im M. et al., 2017, Astron. Telegram, 10481

Jenness T., Currie M. J., Tilanus R. P. J., Cavanagh B., Berry D. S., Leech J., Rizzi L., 2015, MNRAS, 453, 73

Jester S. et al., 2005, AJ, 130, 873

Kilpatrick C. D. et al., 2017, MNRAS, 465, 4650

Kilpatrick C. D. et al., 2018, MNRAS, 473, 4805

Kim H.-J., Yoon S.-C., Koo B.-C., 2015, ApJ, 809, 131

Kochanek C. S., Khan R., Dai X., 2012, ApJ, 759, 20

Kudritzki R.-P., Ho I.-T., Schruba A., Burkert A., Zahid H. J., Bresolin F., Dima G. I., 2015, MNRAS, 450, 342

Kuncarayakti H. et al., 2013, AJ, 146, 30

Lin H., Versteegh A., 2006, in McLean I. S., Iye M., eds, Proc. SPIE Conf. Ser. Vol. 6269, Ground-Based and Airborne Instrumentation for Astronomy. SPIE, Bellingham, p. 62691A

Li W. D. et al., 2000, in Holt S. S., Zhang W. W., eds, AIP Conf. Proc. Vol. 522, Cosmic Explosions. Am. Inst. Phys., New York, p. 103

Li W. et al., 2011, MNRAS, 412, 1441

Maeder A., Meynet G., 1987, A&A, 182, 243

Maund J. R., 2018, MNRAS, 476, 2629

Maund J. R., Ramirez-Ruiz E., 2016, MNRAS, 456, 3175

Maund J. R. et al., 2011, ApJ, 739, L37

Mazzali P. A., Maurer I., Valenti S., Kotak R., Hunter D., 2010, MNRAS, 408.87

Meynet G., Maeder A., 2003, A&A, 404, 975

Meynet G., Maeder A., 2005, A&A, 429, 581

Moffat A. F. J., Seggewiss W., 1977, A&A, 54, 607

Nugis T., Lamers H. J. G. L. M., 2002, A&A, 389, 162

Paxton B., Bildsten L., Dotter A., Herwig F., Lesaffre P., Timmes F., 2011, ApJS, 192, 3

Paxton B. et al., 2013, ApJS, 208, 4

Paxton B. et al., 2015, ApJS, 220, 15

Peacock M. B., Zepf S. E., Finzell T., 2013, ApJ, 769, 126

Podsiadlowski P., Rappaport S., Pfahl E. D., 2002, ApJ, 565, 1107

Poznanski D., Prochaska J. X., Bloom J. S., 2012, MNRAS, 426, 1465

Prochaska J. X., Gawiser E., Wolfe A. M., Cooke J., Gelino D., 2003, ApJS,

Rest A. et al., 2005, ApJ, 634, 1103

Rest A. et al., 2014, ApJ, 795, 44

Sander A., Hamann W.-R., Todt H., 2012, A&A, 540, A144

Schechter P. L., Mateo M., Saha A., 1993, PASP, 105, 1342

Schlafly E. F., Finkbeiner D. P., 2011, ApJ, 737, 103

Shivvers I. et al., 2017, PASP, 129, 054201

Smartt S. J., 2009, ARA&A, 47, 63

Smith N., 2014, ARA&A, 52, 487

Smith L. J., Willis A. J., 1982, MNRAS, 201, 451

Smith N. et al., 2010, AJ, 139, 1451

Smith N., Li W., Silverman J. M., Ganeshalingam M., Filippenko A. V., 2011, MNRAS, 415, 773

Steiner J. E., Oliveira A., 2005, ArXiv Astrophysics e-prints

Stupar M., Parker Q. A., Filipović M. D., 2010, MNRAS, 401, 1760

Taddia F. et al., 2015, A&A, 574, A60

2084 C. D. Kilpatrick et al.

Taubenberger S. et al., 2006, MNRAS, 371, 1459

Tully R. B., Rizzi L., Shaya E. J., Courtois H. M., Makarov D. I., Jacobs B. A., 2009, AJ, 138, 323

Tuthill P. G., Monnier J. D., Danchi W. C., 1999, Nature, 398, 487

Valenti S. et al., 2008, ApJ, 673, L155

Valenti S. et al., 2012, ApJ, 749, L28

van der Hucht K. A., 2001, New A Rev., 45, 135

Van Dyk S. D. et al., 2014, AJ, 147, 37

Van Dyk S. D. et al., 2018, ApJ, 807, 18

Williams P. M., van der Hucht K. A., 2000, MNRAS, 314, 23

Woosley S. E., Langer N., Weaver T. A., 1993, ApJ, 411, 823

Woosley S. E., Eastman R. G., Weaver T. A., Pinto P. A., 1994, ApJ, 429, 300

Yoon S.-C., 2015a, PASA, 32, e015

Yoon S.-C., 2015b, PASA, 32, e015

Yoon S.-C., 2017, MNRAS, 470, 3970

Yoon S.-C., Woosley S. E., Langer N., 2010, ApJ, 725, 940

Yoon S.-C., Gräfener G., Vink J. S., Kozyreva A., Izzard R. G., 2012, A&A, 544, L11